

GlyT1 determines the glycinergic phenotype of amacrine cells in the mouse retina

Volker Eulenburg, Gabriel Knop, Tina Sedmak, Stefanie Schuster, Katharina Hauf, Julia Schneider, Andreas Feigenspan, Aneka Joachimsthaler, Johann Helmut Brandstätter

Angaben zur Veröffentlichung / Publication details:

Eulenburg, Volker, Gabriel Knop, Tina Sedmak, Stefanie Schuster, Katharina Hauf, Julia Schneider, Andreas Feigenspan, Aneka Joachimsthaler, and Johann Helmut Brandstätter. 2018. "GlyT1 determines the glycinergic phenotype of amacrine cells in the mouse retina." *Brain Structure and Function* 223 (7): 3251–66. <https://doi.org/10.1007/s00429-018-1684-3>.



GlyT1 determines the glycinergic phenotype of amacrine cells in the mouse retina

Volker Eulenburg^{1,3}  · Gabriel Knop² · Tina Sedmak² · Stefanie Schuster¹ · Katharina Hauf^{1,3} · Julia Schneider¹ · Andreas Feigenspan² · Anneka Joachimsthaler^{2,4} · Johann Helmut Brandstätter²

Abstract

The amino acid glycine acts as a neurotransmitter at both inhibitory glycinergic and excitatory glutamatergic synapses predominantly in caudal regions of the central nervous system but also in frontal brain regions and the retina. After its presynaptic release and binding to postsynaptic receptors at caudal glycinergic synapses, two high-affinity glycine transporters GlyT1 and GlyT2 remove glycine from the extracellular space. Glycinergic neurons express GlyT2, which is essential for the presynaptic replenishment of the transmitter, while glial-expressed GlyT1 was shown to control the extracellular glycine concentration. Here we show that GlyT1 expressed by glycinergic amacrine cells of the retina does not only contribute to the control of the extracellular glycine concentration in the retina but is also essential for the maintenance of the glycinergic transmitter phenotype of this cell population. Specifically, loss of GlyT1 from the glycinergic AII amacrine cells impairs AII-mediated glycinergic neurotransmission and alters regulation of the extracellular glycine concentration, without changes in the overall distribution and/or size of glycinergic synapses. Taken together, our results suggest that GlyT1 expressed by amacrine cells in the retina combines functions covered by neuronal GlyT2 and glial GlyT1 at caudal glycinergic synapses.

Keywords Glycine · Transmitter · Transporter · GlyT1 · GlyT2 · Retina · Inhibitory neurotransmission · Mouse genetics

Introduction

In the mammalian central nervous system (CNS), GABA and glycine are the principal inhibitory neurotransmitters. In contrast to GABA, which is present in all major brain regions, glycine-dependent inhibition is predominantly found in caudal brain regions and the retina (Legendre 2001). At glycinergic synapses, glycine is loaded into synaptic

vesicles by the vesicular inhibitory amino acid transporter (VIAAT or VGAT) (McIntire et al. 1997; Sagne et al. 1997). After its synaptic release, glycine binds to predominantly postsynaptically localized glycine receptors (GlyRs), thereby enabling the opening of an intrinsic anion channel (Dutertre et al. 2012). In the mature CNS, this results in a hyperpolarization or shunt inhibition of the postsynaptic cell. In addition to its function at inhibitory synapses, glycine has also been described as a coagonist of ionotropic glutamate receptors of the *N*-methyl-D-aspartate (NMDA) subtype (Dingledine et al. 1990). A prerequisite for the dual function of glycine in both inhibitory and excitatory neurotransmission is the precise regulation of its extracellular concentration. This is achieved by two glycine transporters, GlyT1 and GlyT2, which belong to the solute ligand carrier family Slc6a of Na⁺/Cl⁺-dependent neurotransmitter transporters. Although both transporters have been shown to have similar affinities for glycine, they differ in their transport stoichiometry with GlyT1 using 2Na⁺/Cl⁻ and GlyT2 using 3Na⁺/Cl⁻ for the import of one glycine molecule (Roux et al. 2001). This higher driving force for GlyT2-mediated glycine uptake was proposed to allow for sufficiently high presynaptic glycine

✉ Volker Eulenburg
volker.eulenburg@medizin.uni-leipzig.de

¹ Department of Biochemistry and Molecular Medicine, Institute of Biochemistry, Friedrich-Alexander University of Erlangen-Nürnberg, Erlangen, Germany

² Department of Biology, Animal Physiology, Friedrich-Alexander-University of Erlangen-Nürnberg, Erlangen, Germany

³ Present Address: Department of Anesthesiology and Intensive Care Medicine, University of Leipzig, Liebigstrasse 20, 04103 Leipzig, Germany

⁴ Department of Ophthalmology, University Hospital Erlangen, 91054 Erlangen, Germany

concentrations, required for the VIAAT-mediated uptake of glycine into the synaptic vesicles (Supplisson and Roux 2002).

Consistent with its proposed function, GlyT2 localizes to the presynaptic terminals of glycinergic synapses in caudal regions of the brain. Here, GlyT2 is essential for the replenishment of the presynaptic glycine pool and loss of GlyT2 activity results in a breakdown in glycine-dependent inhibition (Gomez et al. 2003b; Rousseau et al. 2008). Consistently, the human GlyT2 gene has been identified as a disease-causing gene for hyperekplexia, a disease that was associated previously with dysfunctional glycinergic inhibition (Eulenburg et al. 2006; Rees et al. 2006).

GlyT1 has been shown to be predominantly expressed by glial cells of brain stem and spinal cord. Additional GlyT1 expression has been reported in presumably glutamatergic neurons (Cubelos et al. 2005; Zafra et al. 1995). Whereas glial GlyT1 controls the extracellular glycine concentration (Eulenburg et al. 2010; Gomez et al. 2003a; Kurolop et al. 2016), the neuronal GlyT1 contributes to the regulation of NMDA receptor activity (Yee et al. 2006). In the mammalian retina, however, GlyT distribution and function appear to be different compared to caudal regions of the CNS. In the retina, GlyT1 is the prevailing glycine transporter and a reliable marker for glycinergic neurons (Haverkamp and Wässle 2000; Pow and Hendrickson 1999; Zafra et al. 1995). Interestingly, however, analysis of mice expressing EGFP under the control of a BAC transgenic GlyT2 promoter revealed reporter expression also in glycinergic amacrine cells in the retina (Dumitrescu et al. 2006; Zeilhofer et al. 2005). These data suggest that both transporters might be coexpressed in glycinergic neurons of the mammalian retina.

In this study, we have analyzed the expression and function of GlyT1 and GlyT2 in the mouse retina by an integrative genetical and electrophysiological approach. By inactivating GlyT1 specifically in glycinergic cells, we show that this transporter is required for the maintenance of the glycinergic phenotype of a major subpopulation of glycinergic amacrine cells in the mammalian retina, the AII amacrine cell. We found that loss of GlyT1 expression in AII amacrine cells resulted not only in a decrease in the intracellular glycine concentration but also in an almost complete loss of glycine-dependent neurotransmission mediated by this cell population. These data establish GlyT1 as a major determinant of glycinergic neurotransmission in the retina.

Materials and methods

Animals

C57BL/6J mice of the indicated genotype were bred at the Institute of Biochemistry and were maintained and

handled in compliance with the local regulations of the Animal Care and Use Committee. Animals had access to water and food ad libitum and were maintained at a 12/12-h light–dark cycle. For all experiments, adult mice of both genders were used. In none of the experiments, differences between male and female mice were observed.

Generation of GlyT1b KI mice

A cDNA fragment encoding for a fusion protein (LucR) of the firefly luciferase (Promega) and FP635 (Origene) was generated by conventional cloning strategies and tested by transient transfection in HEK293 cells. The fusion protein was shown to retain both the luciferase activity as well as the fluorescent properties of the FP635 (data not shown). For the insertion of the cDNA sequence encoding for the fusion protein into the GlyT1 gene, a targeting construct (Fig. 6b) was generated using a strategy combining conventional cloning with recombineering in bacteria (GeneBridges, Germany). Mouse genomic fragments were retrieved from the BAC clone pBACe3.6+rp23-105L12 (BACPAC Resources, Children's Hospital Oakland) that contains large parts of the mouse GlyT1 gene. Here, the LucR-encoding sequence was inserted into the exon 1b of the GlyT1 gene 15 nucleotides downstream of the start codon of GlyT1b. For positive selection, an *flp* recombinase targeting sequence (FRT) flanked PGK–neomycin resistance gene (1.8 kB) was introduced ca. 400 bp downstream of exon 1b. In addition, a herpes simplex virus (HSV) thymidine kinase (2.8 kB) cassette for negative selection was inserted at the 3' end of the targeting construct. For the gene targeting the NotI linearized targeting construct was introduced into Sv129/OlaHasd (E14TG2A) mouse embryonic stem (ES) cells by electroporation and ES cells were selected with FIAU and G418. Individual clones that were both 1-(2-deoxy-2-fluoro-1-D-arabinofuranosyl)-5-iodouracil (FIAU) and geneticin (G418) resistant were isolated and analyzed by Southern blot analysis using *SpeI*/*BglII*-digested genomic DNA and the external probe indicated in Fig. 1a (data not shown). In total, 36 positive clones were identified of which four were injected into C57BL/6J blastocysts. To establish germline transmission of the modified allele, male chimeras obtained from two of these injections were mated with C57BL/6J females. Agouti offsprings were genotyped by PCR and mice carrying the modified allele were mated to Flipper mice (Farley et al. 2000) for excision of the Neo selection cassette. Successful removal of the Neo cassette was verified by Southern blot analysis on *SpeI*/*BglII*-digested tail DNA isolated from tail biopsies using the probe indicated in Fig. 6a. Heterozygous GlyT1b KI mice (GlyT1b^{+/ki}) were mated to obtain homozygous GlyT1b KI mice (GlyT1b^{ki/ki}).

Southern blot analysis

For Southern blot analysis, genomic DNA isolated from tail biopsies was subjected to SpeI/BglII digest. Samples were separated by agarose gel electrophoresis and transferred to a nylon membrane (Hybond N+, GE Healthcare). After crosslinking by UV illumination (1900 $\mu\text{J}/\text{cm}^2$), Southern blots were analyzed using ^{32}P -labeled probes that were generated with the Random-Primed Labeling Kit (Roche). Bound radioactivity was detected using phosphorimager screens (Molecular Dynamics).

RNA isolation

For RNA isolation, animals were rapidly killed by cervical dislocation and decapitation. The respective tissue was rapidly isolated, rinsed briefly in ice-cold PBS and frozen on dry ice for storage. RNA was extracted according to the manufacturer's instructions using the RNA easy Midi kit (Qiagen, Germany) or the E.Z.N.A. Total RNA Kit I (Omega Biotec).

RT-PCR and Northern blot

For RT PCR, RNA isolated from spinal cord, brain stem, heart or retina, respectively, was transcribed to cDNA using an oligo dT primer and the M-MLV reverse transcriptase (Promega) according to the manufacturer's instructions. PCRs for amplification of GlyT1- or GlyT2-specific amplicons were performed with the primers ACC AAGAAGGACCAGAACC and CGATAGCAGAGGTAT GGGAAACG for total GlyT1 and CGACCATTTTGA CTTTTATCCTTTG and CGAGCATACCAACTTCAG CCTC for GlyT2, respectively. GlyT1a-specific amplicons were amplified with the primers GTGCCAAAG GGATGTTGAATGG and CGATAGCAGAGGTATGGG AAACG, GlyT1b-specific amplicons with the primers TATGGCTTCGGCTCAAGG and CGATAGCAGAGG TATGGGAAACG and those specific for actin with the primers GTGACGTTGACATCCGTAAGA and GCC GGACTCATCGTACTCC. Amplicons were analyzed using agarose gel electrophoresis. For northern blot analysis, 20 μg RNA was subjected to 1.5% agarose-formaldehyde gel electrophoresis transferred via capillary transfer to nylon membrane (Hybond N+, GE Healthcare) and detected with DIG-labelled probes using the Northern Starter Kit according to the manufacturer's instructions. cDNA fragments of 271 bp of the GlyT1 cDNA corresponding to the exons 11 and 12 of the GlyT1 gene or 340 bp of the GlyT2 cDNA corresponding to the exons 6–8 of the mouse GlyT2 gene were subcloned into the pGEM vector and used for probe synthesis using the Northern Blot Starter kit (Roche). Northern blots were

hybridized with the respective probes and detected using a CCD-based camera system (Biorad), according to the manufacturer's instructions.

Membrane preparations/Western blots

Animals of the indicated genotype were killed by cervical dislocation and retinae and brain stems were quickly removed and kept on ice. Tissue samples were homogenized in 1 ml membrane isolation buffer (in mM: 330 sucrose, 1 EDTA, 1 PMFS, 10 HEPES, pH 7.4) using a glass Teflon homogenizer. Samples were centrifuged (5 min, 1.000g, 4 °C) to remove tissue debris and the supernatant was transferred to a new tube. Membranes were collected by centrifugation (10 min, 13.000g, 4 °C) and washed twice using Krebs–Henseleit solution (KHP) (in mM: 125 NaCl, 5 KCl, 2.7 CaCl_2 , 1.3 MgCl_2 , 10 Glucose, 25 Tris/Hepes, pH 7.4). Membranes were resuspended in KHP and the protein content was determined using Bradford protein assay (Biorad). Samples were subjected to 8% SDS-PAGE (20 $\mu\text{g}/\text{lane}$) and transferred to nitrocellulose (Hybond P, GE Healthcare). Western blots were analyzed using GlyT1 (Eulenburg et al. 2010) and GlyT2 (Millipore)-specific antibodies, followed by horseradish peroxidase-conjugated secondary antibodies. Blots were incubated with chemiluminescent substrate (Super Signal West Pico, Pierce) and analyzed using a CCD camera-based system (Biorad). Densitometric analysis was performed using Image J 1.50d (Schneider et al. 2012).

Immunohistochemical analysis

For immunohistochemistry, mouse eyes were cut open and cornea and lens were removed. The eyecup containing the retina was fixed for 30 min in 4% paraformaldehyde in PBS at room temperature. Eyecups were washed 3 times for 10 min in cold PBS shaking on ice. For cryoprotection, eyecups were incubated in 10 and 20% sucrose in PBS, for 1 h each and overnight in 30% sucrose in PBS. Vertical cryosections (14 μm) were cut using a cryostat (Leica). Cryosections were dried, washed in PBS 3 times for 10 min, and incubated in blocking solution I [10% (v/v); normal goat serum (NGS), 1% (w/v) bovine serum albumin (BSA), 0.5% (v/v) Triton X-100 in PBS] for 1 h at RT. Sections were incubated overnight with primary antibodies diluted in blocking solution II [3% (v/v) NGS, 1% (w/v) BSA and 0.5% (v/v) Triton X-100 in PBS] at 4 °C in a humid chamber. On the following day, sections were washed 3 times for 10 min with PBS and incubated with the Alexa conjugated secondary antibodies (Invitrogen) diluted in blocking solution II (3% (v/v) NGS, 1% (w/v) BSA and 0.5% (v/v) Triton X-100 in PBS) at RT in a dark humid chamber. Subsequently, sections were washed

3 times for 15 min in PBS and embedded in Aqua Polymount (Polysciences).

The following antibodies were used for immunohistochemical analysis: rat anti-glycine (1:3000, Immunosolutions IG1002), guinea pig anti-GlyT1 (1:50; Schlosser et al. 2015), rabbit anti-GlyT2 (raised against the N-terminal domain 1:200; Gomeza et al. 2003b), guinea pig anti-GlyT2 (raised against the C-terminal domain, 1:1000, AB1773, Merck) rabbit anti-GFP (1:250, A-6455, Invitrogen), rabbit anti-Piccolo6 (1:000, Regus-Leidig et al. 2013), mouse anti-GlyR α 1 (mAB2b; 1:200; Synaptic Systems), and rabbit anti-disabled (1:100, AB5840, Merck Millipore). Secondary antibodies (goat anti-guinea pig, goat anti-rabbit, goat anti-rat and goat anti-mouse conjugated to Alexa488, Alexa568 or Alexa635) were purchased from Invitrogen.

For stainings against GlyR α 1, sections were incubated for 10 min with 4% paraformaldehyde in PBS at 4 °C and washed twice with PBS. Subsequently, before staining sections were washed once with SC buffer {10 mM sodium citrate [0.05% (v/v), Tween-20, pH 8.0] and incubated in SC buffer at 95 °C for 30 min}. Afterwards, the sections were cooled down to RT and processed for staining as indicated above.

Confocal microscopy and image analysis

For analysis of immunohistochemical stainings, a Zeiss Axio Observer 710 confocal laser scanning microscope was used. Images were acquired using 63x oil immersion objective. For image processing, Image J 1.50d and Adobe Photoshop CS4 were used.

Quantification of synaptic cluster densities was done using an in-house particle analysis protocol using Image J 1.50d. In brief, a region of interest was defined in the central region of the IPL of a single confocal image. The image was inverted and digitally filtered using the FT bandpass filter and 2D anisotropic filter option. After background subtraction and thresholding, individual immunofluorescent clusters were counted automatically. The filter settings were optimized individually for recognition of clusters of antibody stainings against Piccolo and GlyR α as a pre- or postsynaptic marker, respectively, and validated by manual counting of total cluster number in individual sections. Number and size of synaptic clusters were analyzed in single optic sections and related to the examined tissue volume. All immunohistochemical samples were treated in parallel and with the same optical and chemical parameters to avoid systematic differences in analysis.

Retina preparation

To dark adapt, mice were kept 2 h in complete darkness. Animals were deeply anesthetized and killed by decapitation.

Retinal whole-mount preparations were performed under infrared (IR) conditions (> 780 nm) using a night vision device. Eyes were enucleated, transferred into oxygenized Ringer's solution (in mM: 125 NaCl, 25 NaHCO₃, 10 D-glucose, 2.5 KCl, 1.6 MgCl₂, 1 CaCl₂) and equilibrated with carbogen (95% O₂, 5% CO₂). Eyes were cut open along the ora serrata; cornea, lens and vitreous were carefully removed with forceps. The retina was isolated by separating the retinal pigment epithelium and cutting the optic nerve.

Recordings of retinal ganglion cells

For electrophysiological recordings, the tissue was perfused with oxygenated Ringer's solution at room temperature (pH 7.4). The retina was kept in a recording chamber with the photoreceptor side down using a nylon grid. The GCL surface was visualized using a CCD camera and a water immersion objective (20x/NA 1.0) on an upright microscope (Zeiss Examiner) under IR conditions. Patch clamp recordings from the ganglion cell layer were established under visual control. Cells were identified by large soma size and fast sodium action potentials. Somatic recordings were performed with a patch-clamp amplifier (HEKA) in voltage clamp mode ($V_m = -70$ mV). Patch clamp pipettes had resistances from 4 to 6 M Ω , yielding series resistances of 10–20 M Ω , which were compensated by a current injection circuit (50%). Intracellular solution contained (in mM: 125 K-gluconate, 10 KCl, 10 HEPES, 0.5 K-EGTA). For pharmacological manipulation, the respective substances were added to the perfusion solution. To block glycinergic neurotransmission 4 μ M strychnine was applied. For blockade of glycine transporter, 10 μ M ALX-5407 (Tocris) was used. From each retina, only one cell was recorded.

Light stimulation

Stimuli were generated on a 7-inch RGB color PC monitor by a custom-made software (QDS, kindly provided by T. Euler, University of Tübingen, Germany). Patterns were projected via the microscope condenser and focused on the outer segments of the photoreceptors. The patched cells were initially characterized using a small-spot-mapping paradigm to discriminate between ON- and OFF-center ganglion cells and to determine the center of the receptive field. Here the retina was successively stimulated by illumination with a series of brief small spots (diameter 50 μ m) dispersed in X- and Y-axes (± 400 μ m) with the position of the recording electrode defined as the center. The center of the receptive field was determined as the X/Y stimulation position that yielded the maximal current response. Here ON-center ganglion cells were characterized by a stimulation-induced pronounced inward-directed current, whereas OFF center ganglion cells showed apparent outward directed currents

Fig. 1 GlyT1 labels glycinergic neurons in the retina. **a** PCR-based analysis for glycine transporter transcripts from RNA and cDNA of wild-type mice ($n=4$); actin-specific primers were used for control. cDNA was generated from RNA isolated from brain stem, spinal cord, heart, and retina. **b** Northern blot analysis of RNA samples from wild-type brain stem, heart, and retina was sequentially probed for GlyT1, GlyT2, and actin expression ($n=3$). **c** Western blot from wild-type retinal and brain stem membrane preparations detected with antibodies specific for GlyT1, GlyT2, and as control GRP75 ($n=3$). **d** Immunohistochemical analysis of vertical retinal sections from wild-type mice ($n=4$). Upper panels: immunolabeling against GlyT1 (red, left side) and GlyT2 (magenta, right side). Of note, there was a prominent membrane-associated GlyT1 immunoreactivity in many cell bodies of the INL and throughout the IPL, but no immunoreactivity with antibodies against GlyT2. Lower panels: double labeling of GlyT1 with antibodies against the neurotransmitter glycine (green). All cell bodies immunoreactive for GlyT1 also showed labeling for glycine. Additionally, weak immunolabeling against glycine was found in cell bodies of the outer parts of the INL. **e, f** Immunohistochemical analysis on vertical retinal sections of ROSY/GlyT2-Cre mice using antibodies specific for GFP (crossreactive for YFP) and glycine (**e**) and for GlyT1 (**f**), respectively (both $n=4$). Note that the majority of glycinergic cells or GlyT1-expressing cells are YFP positive. Scale bars in **d–f** 10 μ m. *OPL* outer plexiform layer, *INL* inner nuclear layer, *IPL* inner plexiform layer, *GCL* ganglion cell layer

upon stimulation of the receptive field center. After identification of the receptive field center, retinal stimulation was performed using a 200- μ m-diameter white spot aimed at the center of the receptive field of the recorded ganglion cells. Maximum stimulus intensities were adjusted to scotopic intensities with neutral density filters. For stimulation of the receptive field center, an intensity of 7 Rh*/rod/s was used. To avoid light adaptation, successive stimulation was separated by 15-s intervals.

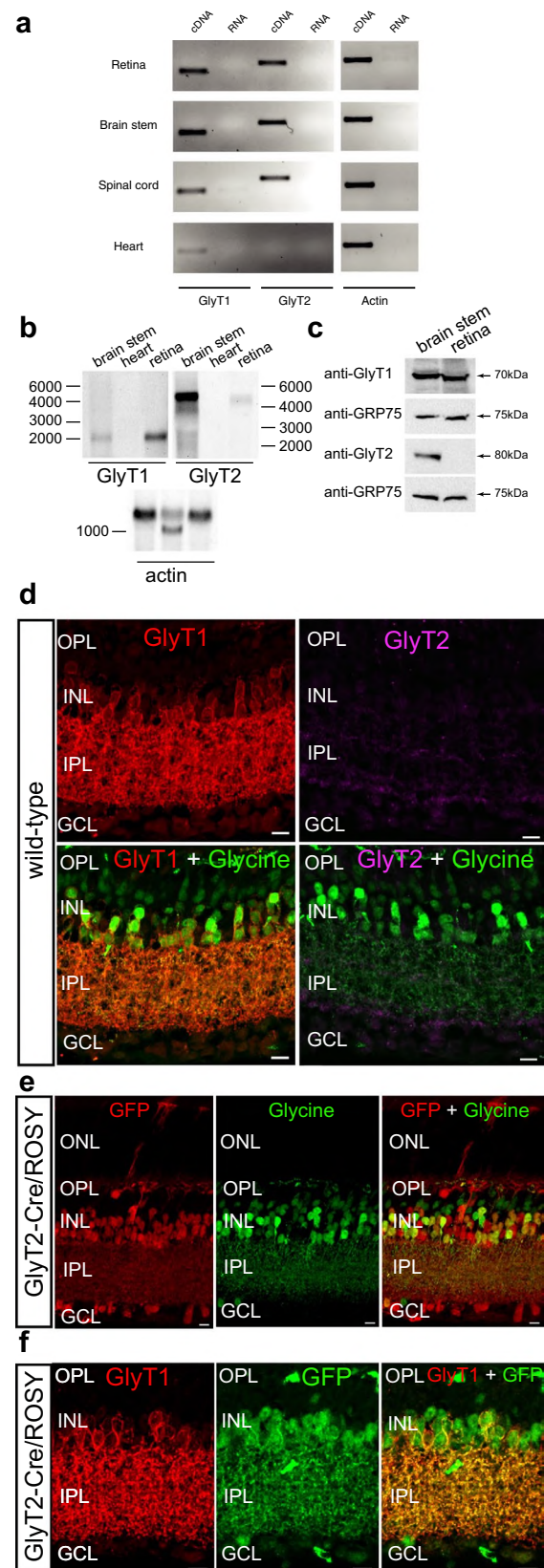
Statistical analysis

Sample sizes were chosen with adequate statistical power on basis of the literature and own experiments. For comparison of two groups, data were analyzed by the non-parametric Mann–Whitney *U* test, if not indicated otherwise. For multiple comparisons, one- or two-way ANOVA followed by Bonferroni's post hoc correction was performed. If not explained otherwise data were presented as box–whisker plots with the whiskers indicating the minimal and maximal data points.

Results

GlyT1 is the prevailing glycine transporter in the mammalian retina

To determine the expression of GlyT1 and GlyT2 in the retina, specific PCRs were performed on cDNA preparations



from wild-type tissue. For both transporters, specific amplicons of the expected size were detected in samples from retina, spinal cord, and brain stem, whereas only a low amount of the GlyT1-specific amplicon was detected in samples from heart. No amplicons were obtained in corresponding RNA samples (Fig. 1a). Successful cDNA synthesis was verified using actin-specific primers, which resulted in strong actin-specific amplicons in all cDNA but none of the RNA samples. To exclude that the signals obtained in the RT-PCR experiments were a result of very low expression, we performed additionally northern blot analyses. Here, signals were obtained with probes specific for GlyT1 and GlyT2 in RNA samples of both brainstem and retina but not heart (Fig. 1b), thus confirming the expression of both GlyTs in retinal samples. To investigate whether GlyT mRNA is also translated into the respective transporter protein in retina, Western blots were performed using GlyT1- and GlyT2-specific antibodies. In brainstem, strong signals were detected with antibodies against both transporters, whereas in the retina only GlyT1 but not GlyT2 immunoreactivity was found (Fig. 1c). Similar results were obtained with a second antibody raised against the C-terminal domain of GlyT2 (data not shown), thus excluding that the lack of GlyT2 immunoreactivity was due to the presence of a different GlyT2 isoform lacking the antigen for the antibody used (i.e., the N-terminal domain). The Western blot results were corroborated by antibody labeling of vertical retinal sections. Here, stainings with a GlyT2-specific antibody did not produce immunofluorescent signals different from stainings with the secondary antibodies alone (Fig. 1d and data not shown). Double-labeling of retinal sections with an anti-GlyT1 and an anti-glycine antibody revealed that all GlyT1 immunoreactive cells were also labeled for glycine, most likely representing the entire glycinergic cell population of the retina (Fig. 1d). In addition, a second cell population with their cell bodies located in the outer half of the inner nuclear layer (INL) showed weak glycine immunoreactivity but lacked a GlyT1-specific immunoreactive signal. These cells most likely correspond to glutamatergic ON-cone bipolar cells, which have been shown to be coupled to glycinergic AII amacrine cells via gap junctions, and receiving the glycine via diffusion from AII amacrine cells (Vaney et al. 1998).

GlyT1 is essential to maintain high intracellular glycine concentrations in glycinergic amacrine cells of the retina

Previous findings have shown GlyT2 promoter activity in a major subpopulation of retinal GABAergic and also glycinergic amacrine cells (Zeilhofer et al. 2005). Therefore, we tested whether Cre recombinase expressed under the control of a BAC transgenic GlyT2 promoter fragment permits an efficient genetic manipulation of glycinergic cells in the

retina. This promoter fragment was shown previously to allow for a specific genetic manipulation of glycinergic cells in brainstem and spinal cord (Ishihara et al. 2010). Indeed, analysis of GlyT2-Cre/ROSA 26-YFP Cre reporter mice revealed YFP-expressing cells in the inner nuclear layer and ganglion cell layer, consistent with Cre expression in a large subset of retinal amacrine cells. Double labeling with antibodies against glycine and GlyT1 showed that a majority of glycinergic cells were YFP positive and expressed GlyT1 (Fig. 1f).

To eliminate the function of GlyT1 in these cells, GlyT2-Cre mice were mated with mice carrying a modified GlyT1 allele that can efficiently be inactivated by expression of Cre recombinase (GlyT1^{fl/fl}) (Eulenburg et al. 2010). GlyT1 expression in retina and brain stem was subsequently analyzed in membrane preparations using Western blot probed with GlyT1-specific antibodies. In samples derived from GlyT1^{fl/fl}/GlyT2-Cre (GlyT1^{GlyT2-Cre}) retinæ a significant reduction in GlyT1 expression by more than 60% was found, as compared to samples from wild-type littermates ($100 \pm 9\%$, vs. $36 \pm 8\%$; $n=4$ samples from different animals per genotype $p < 0.01$, Mann–Whitney U test). In brain stem samples, no difference in GlyT1 expression (Fig. 2a, b, $100 \pm 21\%$ vs. $107 \pm 14\%$; $n=6$ samples from different animals per genotype, $p > 0.8$, Mann–Whitney U test) or GlyT2 expression (Fig. 2a, b, 100 ± 11 vs. $102 \pm 12\%$; $n=6$ samples from different animals per genotype, $p > 0.7$, Mann–Whitney U -test) was detected between the genotypes. In addition, no change in GlyT2 expression was found in membrane preparations from brainstem samples (Fig. 2a, c, $100 \pm 12\%$ vs. $97 \pm 11\%$, $n=6$ samples from different animals per genotype).

Immunohistochemical analysis using GlyT1-specific antibodies revealed a loss of GlyT1 immunoreactivity predominantly in cells with cell bodies positioned close to the border of the INL and the inner plexiform layer (IPL) in GlyT1^{GlyT2-Cre} mice (Fig. 2d). Quantification of GlyT1-immunoreactive cells in the INL of GlyT1^{GlyT2-Cre} mice revealed a reduction by almost 70% as compared to wild-type retina (Fig. 2e, 31.2 ± 8.8 and 11.2 ± 3.5 GlyT1 immunoreactive cells per 200 μm retina in the INL for wild-type and GlyT1^{GlyT2-Cre}, respectively; $n=9$ sections from 4 different animals per genotype; $p < 0.01$, Mann–Whitney U test). Consistent with our Western blot data, no change in the GlyT1 and GlyT2 immunoreactivity was found in other brain regions, i.e., spinal cord (Fig. 2f) or brain stem (data not shown). In retinal sections, double-labeling experiments using glycine and GlyT1-specific antibodies showed a significant reduction in the number of cells showing GlyT1-immunoreactivity in GlyT1^{GlyT2-Cre} mice (Fig. 3a, b). Additionally, fewer cells showing strong glycine immunoreactivity and no cells showing weak glycine immunoreactivity were observed in the INL of

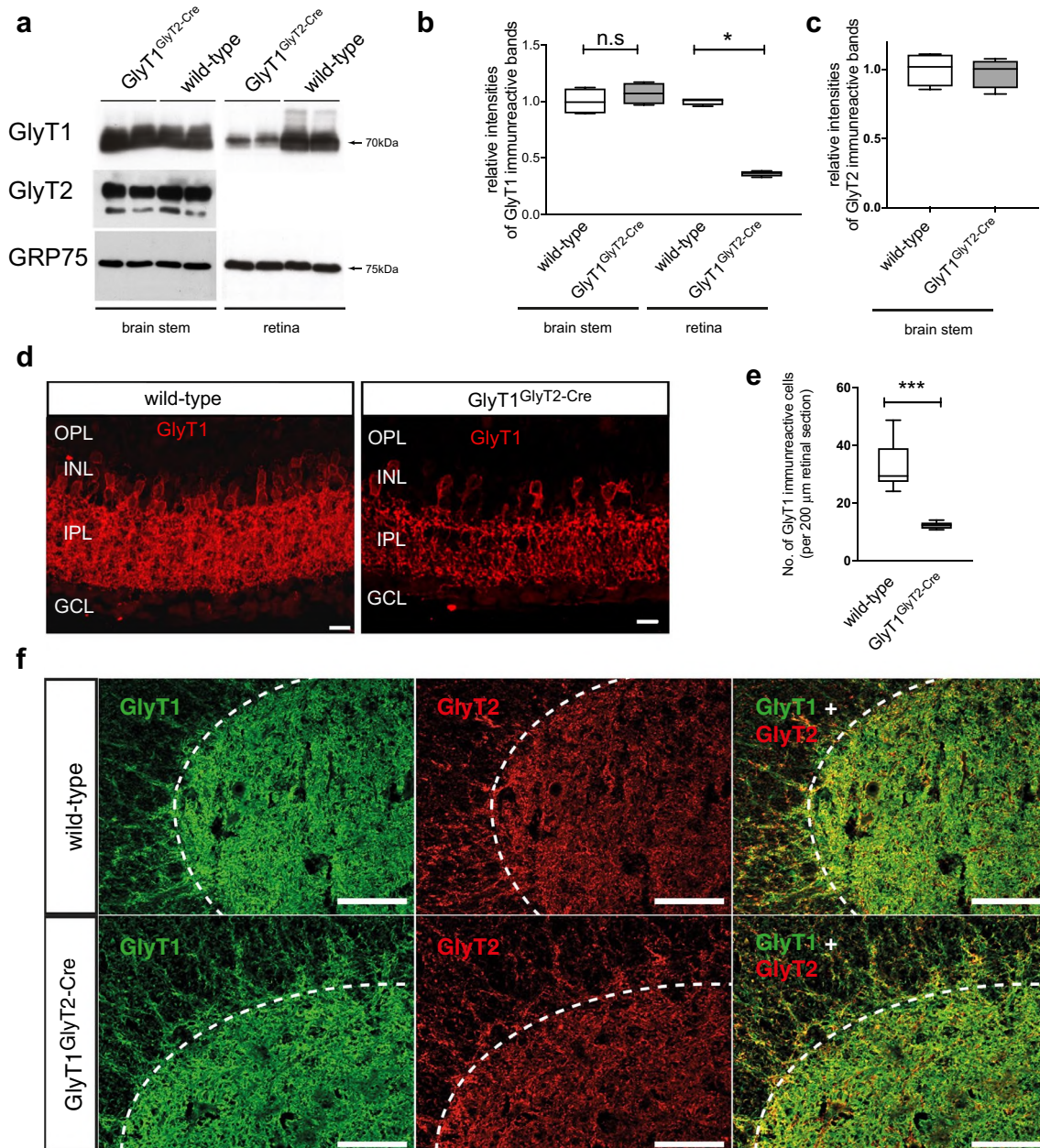


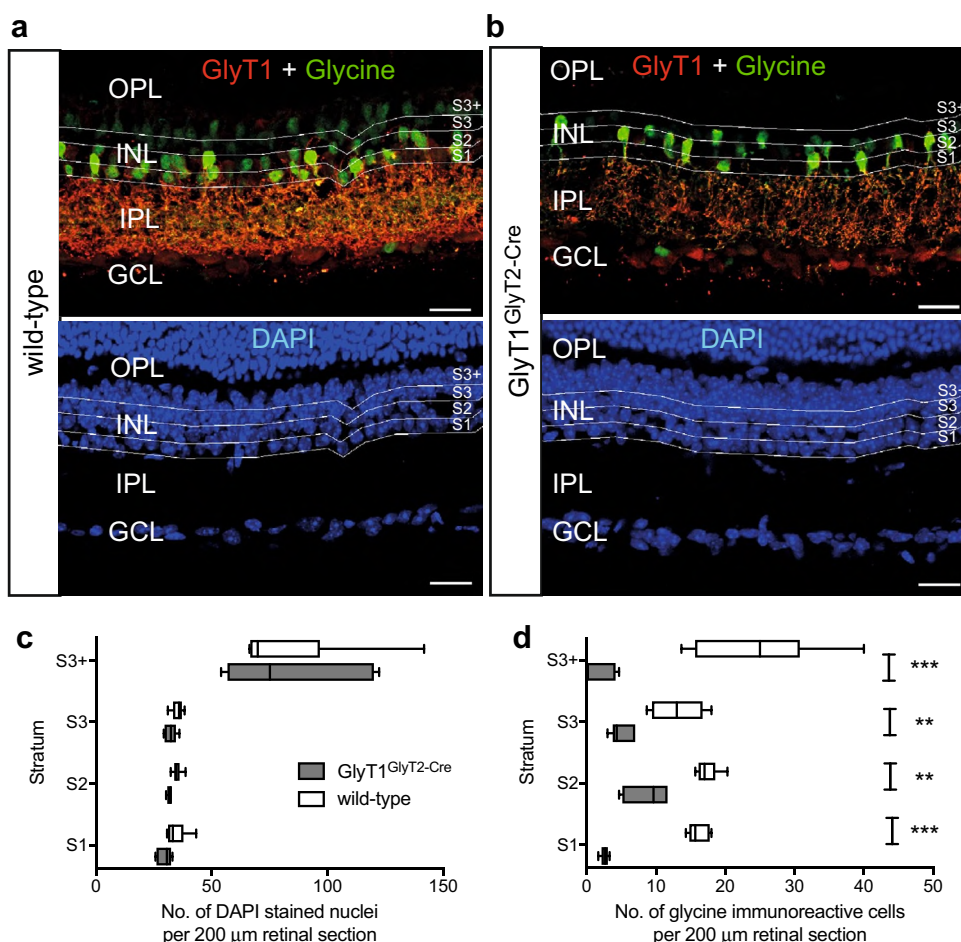
Fig. 2 GlyT1^{GlyT2-Cre} mice show an efficient inactivation of GlyT1 expression in a major glycinergic amacrine cell population. **a** Western blot analysis from membrane preparations derived from retina and brain stem of two different GlyT1^{GlyT2-Cre} mice and wild-type littermates (GlyT1^{fl/fl}) using GlyT1-specific antibodies ($n=6$ per genotype). **b** Densitometric quantification of the GlyT1 immunoreactive band in relation to the GRP75 immunoreactive band on Western blots of brain stem and retinal membrane preparations, respectively ($n=6$ per genotype). **c** Densitometric quantification of the GlyT2 immunoreactive band in relation to the GRP75 immunoreactive band from Western blots of brain stem membrane preparations ($n=6$ per

genotype). **d** Immunohistochemical analysis of vertical retinal sections from GlyT1^{GlyT2-Cre} mice and wild-type littermates using GlyT1-specific antibodies ($n=9$ from 4 different animals per genotype). **e** Number of GlyT1-immunoreactive cells in GlyT1^{GlyT2-Cre} mice and wild-type littermates per 200 μm retinal section ($n=9$ from 4 different animals per genotype). **f** Immunohistochemical analysis of spinal cord sections of wild-type and GlyT1^{GlyT2-Cre} mice using GlyT1- and GlyT2-specific antibodies ($n=9$ from 4 different animals per genotype). Scale bars in **(d)** 10 μm and in **(f)** 100 μm (* $p < 0.05$; *** $p < 0.001$)

GlyT1^{GlyT2-Cre} mice (Fig. 3a, b). Strata-specific quantification of DAPI-stained cell somata revealed that overall cell numbers were not affected (Fig. 3c, $n=9$ sections

from 6 different animals per genotype). The number of the glycine immunoreactive cells was reduced in all strata analyzed with the strongest reduction in the outer part of

Fig. 3 Inactivation of GlyT1 expression results in a loss of the glycinergic phenotype in glycinergic amacrine cells. **a**, **b** Comparison of GlyT1- and glycine-immunoreactivity in vertical retinal sections from GlyT1^{GlyT2-Cre} mice and wild-type littermates ($n=9$ sections from 6 animals for each genotype). For orientation and control, DAPI staining was used to visualize the nuclei. For quantitative analysis, the IPL was divided into 4 strata based on the positions of the cell bodies (cell layers 1–3 or more than 3 cell layers away from the IPL/INL boundary, marked S1–S3, S3+, respectively). **c**, **d** Strata-specific quantification of cell numbers based on DAPI fluorescence (**c**) and on glycine immunoreactivity (**d**) ($n=9$ sections from 6 animals per genotype). Note the almost complete loss of glycine immunoreactive cells in S3+. Scale bar in (**a**, **b**) 20 μm (** $p < 0.01$; *** $p < 0.001$, Mann–Whitney U test)



the INL, more than 3 cell layers away from the INL/IPL border (Fig. 3d, $n=9$ section from 6 different animals per genotype). In this region, ON-bipolar cells are located, which are coupled by gap junctions with glycinergic AII and A8 amacrine cells (Lee et al. 2015; Vaney et al. 1998) allowing diffusion of glycine from these amacrine cells to the bipolar cells. The loss of glycine immunoreactivity in the bipolar cells suggests that in GlyT1^{GlyT2-Cre} mice, among others AII amacrine cells have lost their glycinergic phenotype. To test this hypothesis, sections from wild-type and GlyT1^{GlyT2-Cre} retinæ were analyzed for disabled immunoreactivity, a reliable marker of AII amacrine cells (Lee et al. 2004). In both genotypes, similar densities of amacrine cells labeled for disabled were found (Fig. 4a, b; 7.2 ± 2.2 and 7.8 ± 1.9 disabled immunoreactive cells/200 μm retinal section from wild-type and GlyT1^{GlyT2-Cre} mice, respectively, $n=9$ sections from 5 animals per genotype). Importantly, whereas clear membrane-associated GlyT1 immunoreactivity was observed in all disabled-positive cells in wild-type retina, no GlyT1 immunoreactivity was found in disabled-positive cells in GlyT1^{GlyT2-Cre} retina (Fig. 4a, b, $n=9$ sections from sections of 5 different animals, per genotype; more than 70

cells analyzed per genotype). These results demonstrate that AII amacrine cells had lost GlyT1 expression in GlyT1^{GlyT2-cre} mice.

To determine whether this loss of the glycinergic phenotype in a major population of amacrine cells is accompanied by synaptic changes in the IPL, we performed immunohistochemical stainings against specific synaptic marker proteins. To detect changes in synapse density or size, the presynaptic protein Piccolo (Dick et al. 2001) was analyzed. No significant differences in the overall cluster density ($36.6 \pm 2.1/100 \mu\text{m}^2$ vs. $39.8 \pm 6.1/100 \mu\text{m}^2$, for wild-type and GlyT1^{GlyT2-Cre} samples, respectively; $n=10$ retinal sections from 6 different animals per genotype, $p > 0.1$, Mann–Whitney U test) and cluster size distribution of Piccolo immunoreactivity in samples derived from wild-type and GlyT1^{GlyT2-Cre} mice were observed (Fig. 4c, d).

To determine possible differences in glycinergic synapse density, a similar analysis was performed with a GlyR $\alpha 1$ -specific antibody (mAB2b) (Pfeiffer et al. 1984). Again, no significant differences in cluster density ($55.9 \pm 4.1/100 \mu\text{m}^2$ ($n=8$ retinal sections from 6 different animals) vs. $55.1 \pm 3.0/100 \mu\text{m}^2$ ($n=11$ retinal sections from 6 different animals) for wild-type and GlyT1^{GlyT2-Cre} samples,

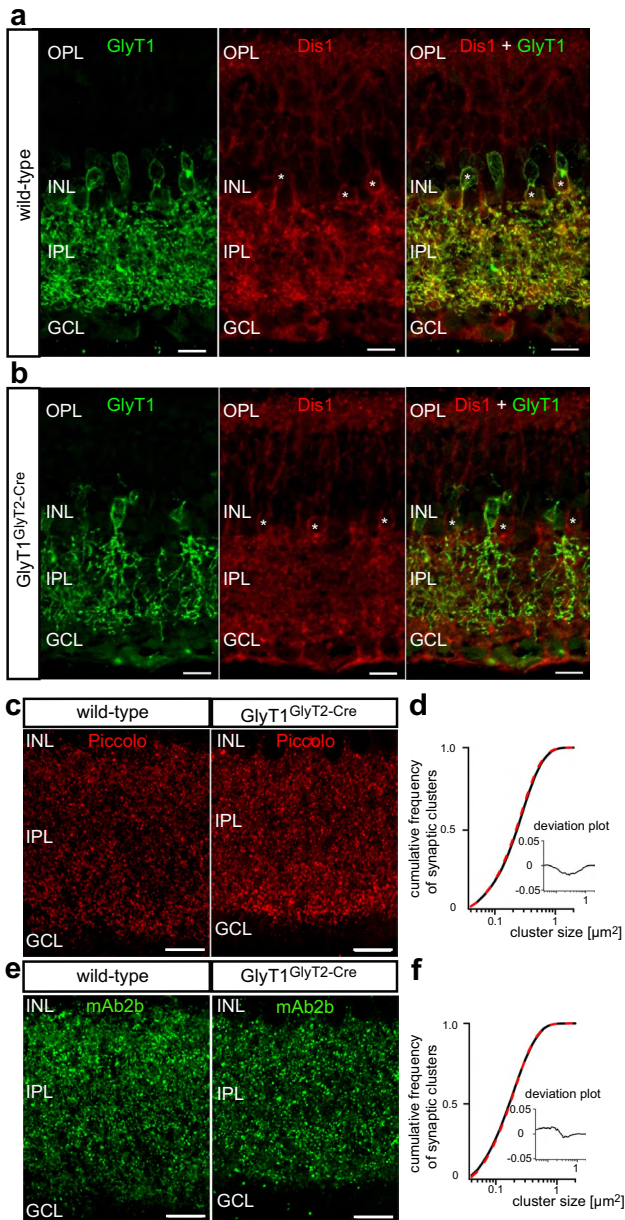


Fig. 4 All amacrine cells of GlyT1^{GlyT2-Cre} mice lose their glycinergic phenotype. **a, b** Double labeling for GlyT1 and disabled (Dis1) in vertical retinal sections from wild-type mice (**a**) and GlyT1^{GlyT2-Cre} mice (**b**) ($n=9$ sections from 5 animals per genotype). Note that in wild-type mice disabled-immunoreactive cells (asterisks) always show membrane-associated labeling for GlyT1, which is lost in preparations from GlyT1^{GlyT2-Cre} animals. **c** Immunolabeling for Piccolo in the IPL of mice with the indicated genotype. **d** Normalized cumulative quantification of Piccolo immunoreactive cluster size distribution within wild-type and GlyT1^{GlyT2-Cre} IPLs (black trace: wild-type; red trace: GlyT1^{GlyT2-Cre}). Inset: deviation plot showing only minor differences between both preparations with maximum deviation below 3% (24,554 and 25,096 clusters for wild-type and GlyT1^{GlyT2-Cre}, respectively, counted from $n=11$ sections of 6 different animals). **e** Immunolabeling for the glycine receptor subunit $\alpha 1$ (GlyR $\alpha 1$; mAb2b) in the IPL of wild-type and GlyT1^{GlyT2-Cre} mice. **f** Normalized cumulative quantification of GlyR $\alpha 1$ -synaptic cluster size distribution (black trace: wild-type; red trace: GlyT1^{GlyT2-Cre}). Inset: deviation plot showing only minor differences between the two mouse strains with a maximum deviation below 2% (57,779 and 60,717 clusters for wild-type and GlyT1^{GlyT2-Cre}, respectively, counted from 8 sections from 6 different animals per genotype). Scale bars in (**a–c**, **e**) 10 μm

respectively; $p > 0.5$, Mann–Whitney U test) and cluster size distribution of the GlyR $\alpha 1$ immunoreactivity were observed between genotypes (Fig. 4e, f). These data demonstrate that the loss of GlyT1 expression in a major glycinergic amacrine cell population did not result in general changes in the synapse distribution within the IPL.

GlyT1 is a major determinant of glycinergic neurotransmission in the retina

To characterize the functional consequences of reduced glycine content in glycinergic AII amacrine cells on retinal processing, we analyzed the electrophysiological response of retinal ganglion cells while stimulating signaling pathways mediated via AII amacrine cells. We, therefore, focused on the scotopic rod pathway (Fig. 5a). Here, the OFF signaling pathway requires glycinergic synapses from AII amacrine cells onto OFF-cone bipolar cells or directly onto OFF-ganglion cells (OFF-GCs), whereas the ON signaling pathway depends on gap junctional signaling between AII amacrine cells and ON-cone bipolar cells (Nelson et al. 1978; Pourcho and Goebel 1985). To monitor signal output from both pathways, currents elicited by low-intensity light were recorded from retinal ganglion cells in the whole cell configuration of the voltage-clamp technique. Using a small-spot mapping paradigm, large ganglion cells with receptive field centers (RFC) of either ON or OFF type were identified. For all experiments, dark-adapted retinal whole-mount preparations were used, with the stimulation centered on the RFC. In voltage-clamp recordings (holding potential $V_m = -70$ mV), ON-ganglion cells (ON-GCs) showed an inward current in response to presentation of a 200- μm -diameter light spot. Consistent with the low scotopic ON light response being transduced by an electrical synapse (Maxeiner et al. 2005), pharmacological blockade with the GlyR antagonist strychnine did not result in a marked change in the light-induced current (Fig. 5b, d, e; rel. peak amplitude: 1.00 ± 0.1 vs. 1.13 ± 0.14 before and after strychnine treatment, respectively, $n=6$, $p > 0.3$, Wilcoxon paired test; rel. charge transfer: 1.00 ± 0.34 vs. 1.375 ± 0.32 before and after strychnine treatment, respectively, $n=5$, $p > 0.4$, Wilcoxon paired test). In contrast, OFF-GCs showed a strong outward directed current in response to light stimulation of the RFC. Application of strychnine resulted in an almost complete inhibition of the light-induced current response (Fig. 5c–e; rel. peak amplitude: 1.00 ± 0.3 vs. 0.09 ± 0.06 for before and after strychnine treatment, respectively, $n=4$, $p \leq 0.05$, Wilcoxon paired test; rel. charge transfer: 1.00 ± 0.32 vs. 0.05 ± 0.07 for recordings before and after strychnine treatment, respectively; $n=4$, $p \leq 0.05$, Wilcoxon paired test). This is consistent with a decrease in glutamatergic input from OFF-bipolar cells caused by glycinergic inhibition from AII amacrine cells. Subsequently, the experiments were repeated in mice

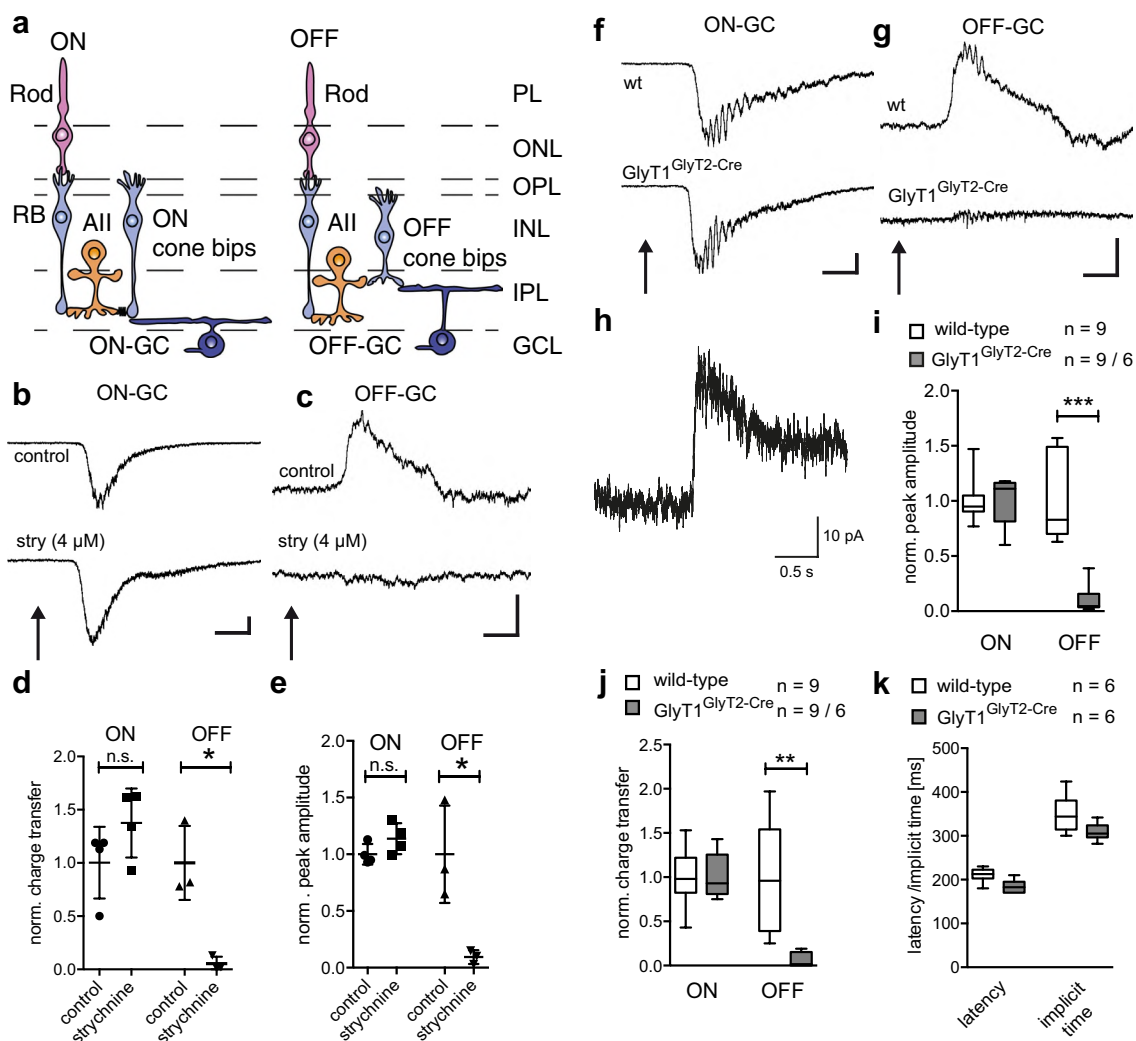


Fig. 5 GlyT1^{GlyT2-Cre} mice show defects in the rod OFF but not ON signaling pathway mediated by AII amacrine cells. **a** Schematic overview of synaptic connectivity relaying scotopic light responses [modified with permission from (Wässle 2004)]. Within the receptive field center (RFC) scotopic rod signals are mediated mainly via rod bipolar cells and AII amacrine cells. AII amacrine cells transmit their signals via gap junctions and glycinergic synapses to the ON and OFF channel, respectively. Cone bipolar cells convey light responses via glutamatergic excitation to ganglion cells. In ON-GCs, illumination of the RFC leads to an increase in cone bipolar cell excitatory input, while in OFF-GCs cone bipolar cell excitatory input is reduced upon light stimulation. **b, c** Example of light-induced currents from mouse retinal ganglion cells with the membrane potential held at -70 mV evoked by a scotopic light spot (diameter $200\ \mu\text{m}$) projected to the RFC (light intensity $7\ \text{Rh}^*/\text{rod/s}$), time of light onset is marked by arrows. Currents from ON-center (**b**) and OFF-center (**c**) ganglion cells recorded before and after application of strychnine ($4\ \mu\text{M}$, 2 min). **d** Normalized light-induced charge transfer before and after strychnine application (values normalized to control, $n=6$ for ON-GCs and $n=5$ for OFF-GCs, respectively. Each cell was derived from

a different retina). **e** Maximum current amplitude before and after strychnine application ($n=6$ for ON-GCs and $n=5$ for OFF-GCs, respectively. Each cell was derived from a different retina). **f, g** Examples of light responses of ON-GCs (**f**) and OFF-GCs (**g**) in wild-type (upper traces) and GlyT1^{GlyT2-Cre} mice (lower traces). Time of light onset is marked by an arrow. **h** Magnified example of the residual current of OFF-GCs observed in retinae from GlyT1^{GlyT2-Cre} mice. **i** Comparison of normalized peak current amplitude in wild-type and GlyT1^{GlyT2-Cre} mice ($n=6$ cells per genotype for ON-GCs and OFF-GCs, respectively). **j** Comparison of the light-induced charge transfer in wild-type and GlyT1^{GlyT2-Cre} mice. Values were normalized to the wild-type amplitudes of ON- and OFF-center-GCs, respectively ($n=6$ cells per genotype for ON-GCs and OFF-GCs, respectively). Vertical bars represent $200\ \text{pA}$ current (b, c, f–h). Horizontal bar represents $200\ \text{ms}$ time. All traces represent a five times average response. **k** Comparison of ON-GC response latency and implicit time in wild-type mice compared to GlyT1^{GlyT2-Cre} mice ($n=6$ cells per genotype for ON-GCs and OFF-GCs, respectively) ($*p < 0.05$; $**p < 0.01$; $***p < 0.001$, Mann–Whitney U test for **h, i**, Wilcoxon test for **d, e**)

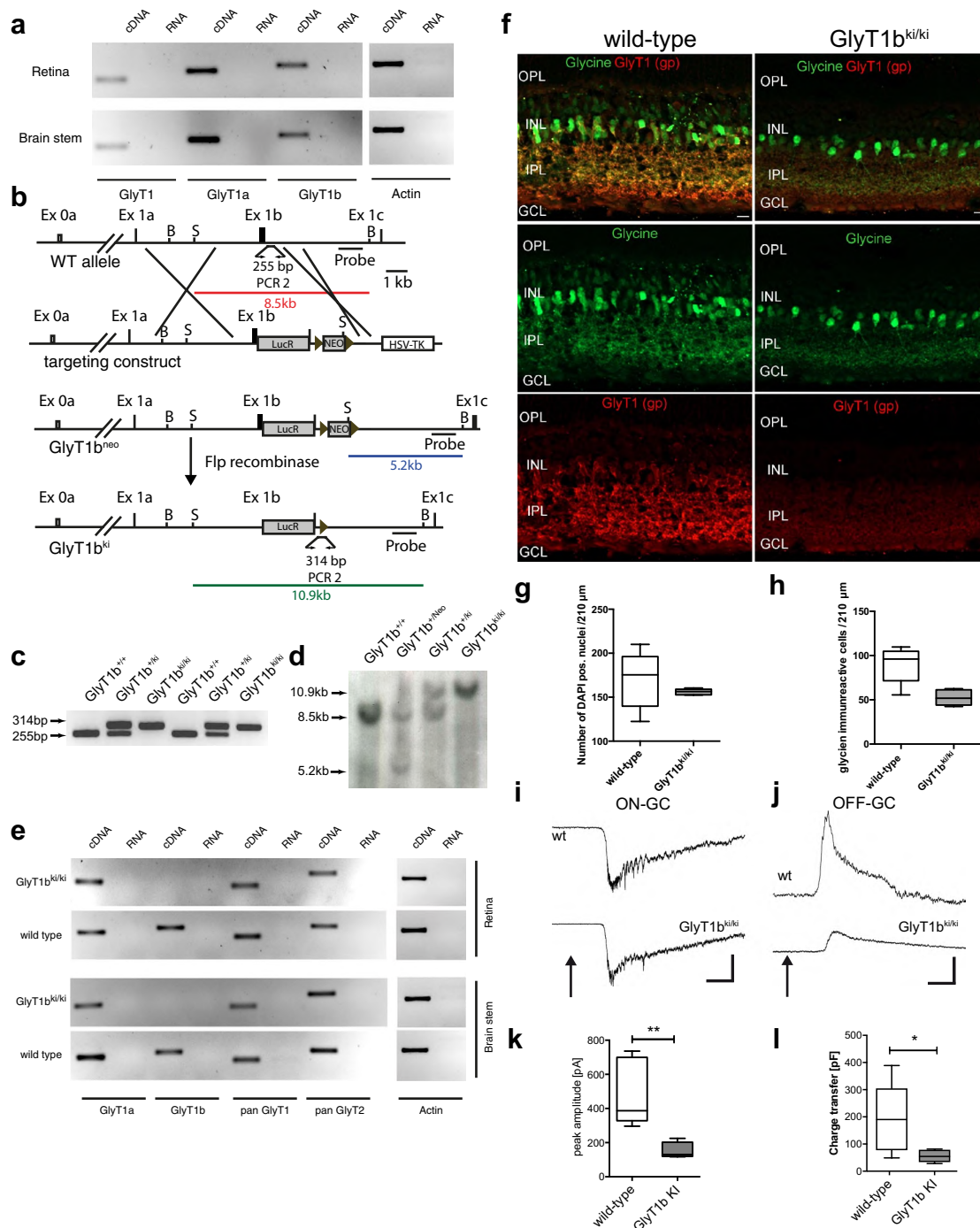
deficient in GlyT1 expression in AII amacrine cells. Here, in ON-GCs the maximal amplitude of the light-induced current response was indistinguishable between genotypes (Fig. 5f, i, j; rel. peak amplitude: 1.00 ± 0.20 vs. 0.99 ± 0.21 for light responses from wild-type and GlyT1^{GlyT2-Cre} retinal preparations, respectively; $n = 9$ cells per genotype, $p > 0.5$, Mann–Whitney U test; rel. charge transfer: 1.00 ± 0.32 vs. 1.01 ± 0.25 for recordings from wild-type and GlyT1^{GlyT2-Cre} retinae, respectively, $n = 9$ cells per genotype, $p > 0.3$, Mann–Whitney U test), although both the implicit time as well as the response latency were reduced (Fig. 5k; latency: 211 ± 17 ms vs. 184 ± 15 ms; $n = 9$ cells per genotype, for light responses recorded from wild-type and GlyT1^{GlyT2-Cre} retina, respectively, $p < 0.05$, Mann–Whitney U test; implicit time: 350 ± 43 ms vs. 309 ± 20 ms; for light responses recorded from wild-type and GlyT1^{GlyT2-Cre} retina, respectively; $n = 9$ cells per genotype, $p > 0.05$, Mann–Whitney U test). In recordings from OFF-GCs from GlyT1^{GlyT2-Cre} mice, however, a more than 80% loss of the light-induced current response was observed (Fig. 5g–i; peak amplitude 1.00 ± 13 vs. 0.10 ± 0.06 for light responses from wild-type ($n = 9$ cells) and GlyT1^{GlyT2-Cre} ($n = 6$ cells) retinal preparations, respectively, $p < 0.01$ Mann–Whitney U test; charge transfer 1.00 ± 61 vs. 0.05 ± 0.09 for light responses from wild-type ($n = 9$ cells) and GlyT1^{GlyT2-Cre} ($n = 6$ cells) retinal preparations, respectively, $p < 0.001$ Mann–Whitney U test).

Although we have not found any significant difference in the density of glycinergic synapses, we cannot exclude that GlyT1 deficiency caused a specific loss of glycinergic synapses formed by the AII amacrine cells. Since we could show that a fraction of GlyT1 expression within the retina is GlyT1b (Fig. 6a), we made use of a newly generated mouse line carrying homozygously an insertion of a luciferase reporter construct downstream of the start codon of GlyT1b (GlyT1b^{ki/ki} mice, Fig. 6b–d). In these mice, a modified GlyT1b mRNA is expressed that does not allow for GlyT1b protein expression. The expression of GlyT1a, however, is predicted to be unaffected. These mice were born at the expected Mendelian ratio and were vital. RT-PCR analysis revealed a slight reduction in GlyT1 expression in both brain stem and retina, and showed a total loss of GlyT1b, but not of GlyT1a expression (Fig. 6e). Immunohistochemical analysis of vertical sections of the retina with a pan-GlyT1 antibody revealed not a complete loss but a more than 80% reduction in GlyT1 protein expression (Fig. 6f). Although the number of cells showing strong glycine immunoreactivity within the INL was significantly reduced, the number of DAPI-positive cells was unchanged (Fig. 6g, h). Electrophysiological recordings of scotopic light responses from ON-GCs of GlyT1b^{ki/ki} and wild-type mice gave comparable results (Fig. 6i; 748 ± 581 pA vs. 652 ± 297 pA for recordings from ON-GC of wild-type and GlyT1b^{ki/ki} retinae, respectively; $n = 6$ for wild-type and 4 for GlyT1b^{ki/ki}).

Recordings of light-induced OFF-GC responses, however, showed a 70% reduction in current amplitudes and charge transfer induced by a low-intensity light stimulus (Fig. 6j–l, $n = 5$ cells per genotype), suggesting a direct correlation of GlyT1 activity with glycine-dependent currents recorded from OFF-GCs. Consistent with previous experiments, the residual current observed was GlyR dependent, since an incubation with strychnine (4 μ M) resulted in an almost complete block of the remaining current ($n = 3$, data not shown). In addition to the reduction in current amplitudes, a tendency for a prolongation of the decay kinetics of the current response was observed (Fig. 6j, and data not shown). These data suggest that GlyT1 might also play a role in terminating the glycine-dependent neurotransmission mediated via AII amacrine cells.

GlyT1 expressed by amacrine cells contributes to the regulation of the extracellular glycine concentration

The contribution of GlyT1 to the control of the extracellular glycine concentration was analyzed by its acute pharmacological blockade with the specific GlyT1 inhibitor ALX5407 (Atkinson et al. 2001). Current amplitudes elicited by scotopic light stimulation measured in recordings from ON-GCs were indistinguishable before and after 30 min superfusion with 10 μ M ALX5407 (Fig. 7a, c, 1.00 ± 0.34 vs. 0.99 ± 0.35 ; $n = 5$, $p > 0.8$, Wilcoxon test). However, a slight acceleration in the early decay time (25% decay time) was observed (Fig. 7d, g, 1.00 ± 0.21 vs. 0.72 ± 0.29 for light responses before and after ALX5407 treatment, respectively; $n = 5$, $p < 0.2$, Wilcoxon test). In contrast, current amplitudes in recordings from OFF-GCs were reduced in response to incubation with ALX5407 (Fig. 7b, c, 1.00 ± 0.39 vs. 0.63 ± 0.19 , before and after ALX5407 treatment, respectively, $n = 5$, $p < 0.05$, Wilcoxon paired test). Scaling of the light-induced currents after ALX5407 treatment to the maximal amplitude observed in the recording before the start of the treatment revealed that inhibition of GlyT1 resulted in a significant change in the decay kinetics of the light-induced current. Although there was no significant change in the fast component of the decay kinetic as illustrated by the 25% decay time (Fig. 7g, 1.00 ± 0.26 vs. 0.95 ± 0.29 ; before and after ALX5407 treatment, respectively, $n = 5$, $p > 0.40$, paired Wilcoxon test), there was a significant increase in the slow component of the decay kinetics as indicated by the 75% decay time (Fig. 7f, 1.00 ± 0.19 vs. 1.67 ± 0.52 before and after ALX5407 treatment, respectively; $n = 5$, $p < 0.05$, Wilcoxon test). These data suggest that GlyT1 is responsible for both the maintenance of a high intracellular glycine pool required for synaptic release, and the clearance of glycine from the synaptic cleft at AII amacrine cell synapses.



Discussion

Glycine transporter expression in the retina

In this study, we explored the expression, distribution, and function of glycine transporters in the mouse retina. Results from RT-PCR and Northern blot analysis demonstrated that similar to the caudal CNS, mRNAs for both glycine transporters, GlyT1 and GlyT2, were present in the retina.

However, in agreement with previous work, GlyT2 protein was not detected in the retina (Pow and Hendrickson 1999). Possible reasons for this discrepancy include translational silencing, e.g., via a miRNA-based mechanism, or rapid degradation of translated GlyT2 protein. Antibody labeling revealed the presence of GlyT1 in most glycinergic amacrine cells, thus confirming previous results showing that GlyT1 is the prevailing glycine transporter in the retina and, therefore, a reliable marker of glycinergic amacrine cells (Pow

Fig. 6 GlyT1b^{ki/ki} mice show reduced expression of GlyT1 and altered strength and kinetics in glycinergic neurotransmission. **a** RT-PCR analysis of RNA preparations of wild-type retina and spinal cord using GlyT1-, GlyT1a- and GlyT1b-specific primer sets. Efficient cDNA synthesis was verified by amplification of an actin-specific amplicon ($n=3$). **b** Gene targeting strategy for the generation of a GlyT1b-LucR knock-in mouse (GlyT1b Ki), LucR reporter is indicated as a grey box, Neo and HSV-TK cassette are indicated as white boxes. Frt sites are displayed as triangles. BglII (B) and SpeI (S) sites as well as the primers used for genotyping (arrows) and the probe used for Southern blot analysis are indicated. **c** PRC-based genotyping on genomic DNA derived from tail biopsies of GlyT1b^{ki} mice with the primers indicated in **b** ($n=3$ per genotype). **c** Southern blot analysis of SpeI/BglII-digested genomic DNA derived from tail biopsies of the mice with the indicated genotype with the probe indicated in **b** ($n=3$ per genotype). **e** RT-PCR analysis of RNA preparations from retina and brainstem of wild-type and GlyT1b^{ki/ki} mice using GlyT1- and GlyT2-specific primers, in addition, primers specific for the GlyT1 isoforms GlyT1a and GlyT1b were used. Efficient cDNA synthesis was verified by amplification of an actin-specific amplicon ($n=3$ per genotype). **f** Double labeling of vertical retinal sections derived from wild-type (left) and GlyT1b^{ki/ki} animals using glycine and GlyT1-specific antibodies ($n=4$ per genotype). **g, h** Quantification of the number of DAPI-positive nuclei (**g**) and glycine immunoreactive cells (**h**) within the IPL of wild-type and GlyT1b^{ki/ki} animals, respectively ($n=8$ section from 4 different animals per genotype). **i** Representative light responses from retinal ON-GC. The top trace shows light-induced currents in wild-type animals and lower trace from GlyT1b^{ki/ki} animals ($n=5$ cells per genotype). **j** Representative current traces from OFF-GC, showing a marked decrease in current amplitude in GlyT1b^{ki/ki} animals (bottom trace) as compared to those from wild-type animals (top trace) ($n=5$ cells per genotype). Light stimulation parameters: 200- μ m-diameter light spot at 7 Rh*/rod/s intensity, centered on the receptive field center of the respective cell. Time of light onset is marked by black arrows. Note that decay kinetics in GlyT1b^{ki/ki} preparations were significantly prolonged. **k, l** Quantification of maximum current amplitude and light-induced charge transfer from OFF-ganglion cells light responses of wild-type animals and GlyT1b^{ki/ki} (grey bars) ($n=4$ cells per genotype). Scale bars in (**f**) 10 μ m. Vertical bars in (**i, j**) represent 200 pA current. Horizontal bars represent 200 ms time (** $p < 0.01$; *** $p < 0.001$; Mann-Whitney U test)

and Hendrickson 2000). Consistent with GlyT2 promoter activity in the retina, analysis of GlyT2-Cre/ROSA 26-YFP reporter mice revealed a large population of YFP-expressing cells in the INL of the retina. Immunohistochemical experiments showed that reporter-expressing cells not only included many glycinergic amacrine cells but also some non-glycinergic cells within the INL. These findings are in line with previous reports from mice expressing EGFP-reporter under control of a BAC transgenic GlyT2-promoter fragment, showing that GlyT2-promoter activity is a reliable marker of glycinergic amacrine cells although some reporter expression was observed in cells containing GABA as a neurotransmitter (Dumitrescu et al. 2006). Consistent with a glycinergic phenotype, the majority of GFP-expressing cells also showed GlyT1 immunoreactivity. There were, however, also some GlyT1-positive cells that did not show any reporter expression. Whether this is due to insufficient levels of Cre expression in these cells (e.g., due to heterogeneity of

transgene expression) or due to (developmental) heterogeneity of the glycinergic amacrine cells themselves is unclear at present and deserves further investigation. This, however, is clearly beyond the scope of this manuscript.

Interestingly, a clear difference in the pattern of GlyT1 inactivation was observed in the retina of GlyT1^{GlyT2-Cre} mice and GlyT1b KI mice. Here, glycinergic amacrine cells from GlyT1b^{ki/ki} mice showed a homogenous loss of GlyT1 expression to ca. 20% of that observed in sections of wild-type animals, suggesting that ca. 20% of the total GlyT1 activity in the retina are carried by GlyT1a, whereas the majority is carried by GlyT1b. Indeed, RT-PCR analysis revealed that in the retina, both GlyT1a and GlyT1b were expressed (Fig. 6e). Taken together these data suggest that in glycinergic amacrine cells, both GlyT1a and GlyT1b synergistically mediate the high-affinity glycine uptake. This contrasts with findings from GlyT1^{GlyT2-cre} mice. Here the loss of GlyT1 expression is solely determined by the expression of Cre recombinase in amacrine cells showing GlyT2 promoter activity.

GlyT1^{GlyT2-Cre} mice show retina-specific ablation of GlyT1 expression

In retinae of GlyT1^{GlyT2-Cre} mice, we found an almost 70% reduction in the number of GlyT1-immunoreactive cells as compared to wild-type controls, whereas in samples from other brain regions, e.g., spinal cord, no difference in the distribution of GlyT1 immunoreactivity was observed. These findings demonstrate that in these brain regions GlyT1 is not expressed in glycinergic neurons (Zafra et al. 1995), thus confirming that GlyT1^{GlyT2-Cre} mice carry a retina-specific ablation of GlyT1 expression. In the retina, the loss of GlyT1 resulted in a reduction in the number of glycine-immunoreactive cells in the INL. All remaining GlyT1-positive retinal neurons sustained a high intracellular glycine concentration as indicated by strong glycine immunoreactivity. These findings are consistent with the idea that GlyT1 is essential for the maintenance of the glycinergic “phenotype” in the retina. This contrasts findings from brain stem and spinal cord. Here, exclusively GlyT2, but not GlyT1, was found to be required for the maintenance of high intracellular glycine concentrations in glycinergic neurons (Gomez et al. 2003b; Latal et al. 2010). The loss of the weak glycine immunoreactivity in the bipolar cells of GlyT1^{GlyT2-Cre} mice suggests that glycinergic amacrine cells that are gap junction coupled to bipolar cells are affected by GlyT1 deletion. These include, in addition to the A8 amacrine cells (Lee et al. 2015), the AII amacrine cells (Rice and Curran 2000).

Comparable to the effects observed after GlyT2 deficiency in brain stem (Gomez et al. 2003b; Latal et al. 2010), no significant change in the synaptic cluster distribution or the overall distribution of inhibitory synapses was found in

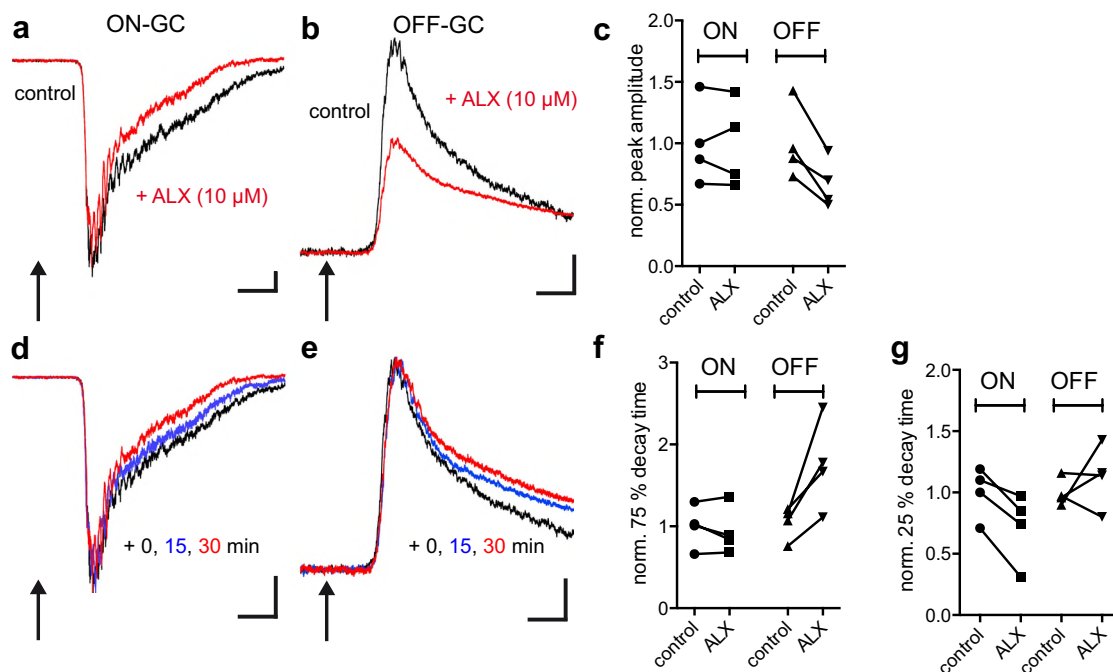


Fig. 7 Pharmacological inhibition of GlyT1 in wild-type retinal preparations reduces in the OFF-GC current amplitude and prolongates of the decay kinetics. GC responses to a scotopic light spot (diameter 200 μm) projected to the receptive field center (cells held at -70 mV, light intensity 7 $\text{Rh}^*/\text{rod/s}$, time of light onset marked by arrows). **a, b** Example recording of ON-GC (**a**) and OFF-GC (**b**) under control conditions (black lines) and after 30 min ALX5407 application (10 μM , red lines). **c** Normalized peak current amplitude before and after 30 min of ALX5407 (10 μM) application. **d, e** Effect of glycine transporter blockade on decay kinetics of light-induced currents. Examples of normalized currents recorded from an ON-GC (**d**) and an OFF-GC (**e**) at start (black traces), after 15 min (blue traces) and

after 30 min (red traces) of ALX5407 (10 μM) application. All traces were scaled to the maximal amplitude of the pre-ALX condition. **f** Quantification of the 75% decay time before and after 30 min of ALX5407 application ($n=5$ cells per genotype for ON and OFF-GCs respectively). **g** Quantification of the 25% decay time before and after 30 min of ALX application ($n=5$ for ON and OFF-GC per genotype, respectively). Vertical bars represent 200 pA current (**a, b**) and 20% normalized current (**d, e**). Values were normalized to the mean initial amplitudes of ON- and OFF-center GC, respectively. Horizontal bar represents a five times average response (* $p < 0.05$, Mann-Whitney U test)

GlyT1^{GlyT2-Cre} retinae, suggesting that GlyT1 deficiency does not result in major adaptive changes in retinal synaptic circuitry. The density of Piccolo immunoreactive clusters found in individual optical sections from our retinal preparations, however, was relatively low as compared to the literature (Dick et al. 2001). This results probably from technical differences like altered thickness of the optical sections and/or the staining procedure that might affect the detection limit.

GlyT1 deficiency in AII amacrine cells impairs glycinergic neurotransmission

Electrophysiological recordings from OFF-GCs showed an almost complete loss of scotopic light-induced responses, similar to recordings from wild-type retinae after blockage of glycinergic neurotransmission with strychnine. These findings are consistent with an almost complete abolishment of glycine-dependent neurotransmission via the AII amacrine cells in GlyT1^{GlyT2-Cre} retinae (Protti et al. 2005).

Interestingly, light-induced responses from ON-GCs were similar to those observed in wild-type recordings, despite minor changes in kinetics. Since this pathway depends on gap junctional coupling between AII amacrine and ON-cone bipolar cells (Deans et al. 2002), these findings confirm that AII amacrine cells were still present in GlyT1-deficient animals, but they have lost their glycinergic phenotype.

GlyT1 expressed by amacrine cells contributes to the control of the extracellular glycine concentration

Both our electrophysiological experiments on GlyT1b KI retinae as well as pharmacological blockage of GlyT1 in wild-type retinal whole mounts are consistent with the idea that the loss of glycinergic inhibition was not due to a loss of glycinergic synapses in AII amacrine cells but was a direct consequence of the reduced glycine reuptake capacity of AII amacrine cells. Especially the gradual loss of

glycinergic inhibition via the AII amacrine cells observed after inhibition of GlyT1 by ALX5407 clearly confirms that the maintenance of a high intracellular glycine concentration is dependent on glycine transport from the extracellular space via GlyT1 and not on de novo synthesis (Pow 1998). Interestingly, the blockade of GlyT1 does not result in the complete loss of glycine-dependent neurotransmission within the timeframe of the experiment. This is most likely due to the large vesicle pool size and residual glycine in the presynaptic terminals of the AII amacrine cells still available for glycinergic neurotransmission. In addition to the changed current amplitudes, also changes in the decay kinetics of the light-induced currents were observed. Whereas the fast component of the decay kinetics, most likely driven by diffusion, was unchanged, the slow component of the decay kinetic was significantly prolonged. These findings suggest that in OFF-light responses GlyT1 is not only required for the replenishment of the presynaptic transmitter pool but also contributes to the clearance of glycine from the synaptic cleft. In brain stem, this function has been attributed to GlyT1 expressed by glial cells (Eulenburg et al. 2010). Thus, GlyT1 expressed by glycinergic amacrine cells combines functions which are performed by glial GlyT1 and neuronal GlyT2 in other regions of the CNS (Gomez et al. 2003a, b). Since Müller glial cells do not show significant GlyT1 expression, the turnover of glycine at retinal glycinergic synapses appears to be solely dependent on neuronally expressed transporters. Whether this is due to the spatial organization of the glycinergic synapses in the retina and their effect on neurotransmitter diffusion and/or clearance is not clear at present.

Our findings that a pharmacological block of GlyT1 by ALX5407 resulted in a time-dependent reduction of glycine-dependent input to OFF-GCs demonstrate that GlyT1 expressed by retinal amacrine cells is sufficient to maintain high intracellular glycine levels required for efficient glycine-dependent neurotransmission. Thus, a transporter that has been predicted to work close to equilibrium (Supplisson and Roux 2002) suffices to maintain a sufficiently high millimolar intracellular glycine concentration in presynaptic terminals for VIAAT-mediated vesicle loading.

As a consequence, the requirement for the use of GlyT2, i.e., a transporter with a higher driving force for glycine uptake as compared to GlyT1, for the presynaptic glycine accumulation (Roux and Supplisson 2000; Supplisson and Roux 2002) at caudal glycinergic synapses cannot be explained by the low affinity of VIAAT for glycine. Alternatively, GlyT2 might be required to lower the extracellular glycine concentration to induce glial GlyT1 to reverse, thus triggering the transporter-mediated release of glycine from glial cells in close proximity to glycinergic synapses. This mechanism might allow for an efficient transfer of glycine from glial cells to glycinergic neurons. In the retina,

however, only neurons carry high-affinity glycine transporters, thus making the higher driving force of GlyT2 for glycine import dispensable.

In summary, our results show that in contrast to brain stem and spinal cord, GlyT1 and not GlyT2 is essential for the replenishment of the presynaptic glycine pool in retinal AII amacrine cells and is a major determinant of the glycinergic phenotype of this cell population. Moreover, we show that GlyT1 contributes to the regulation of the extracellular glycine concentration thus converging functions distributed to neuronal and glial glycine transporters, respectively, in other brain regions. Future work will have to unravel how these differences affect transmitter turnover and synapse properties.

Acknowledgements The authors thank Renate Kühnhauser, Marina Kleber and Freya Boggasch for excellent technical assistance. Parts of this work were supported by Grants from the Deutsche Forschungsgemeinschaft to V. E. (EU110/3-1 and EU110/6-1).

Author contributions VE, GK, and JHB designed experiments. GK, TS, SS, KH, JS, AJ, AF, and VE performed experiments. GK, TS, KH, JHB, AF, and VE analyzed data, VE wrote the manuscript with comments from all coauthors. All authors agreed on the final version of the manuscript.

Compliance with ethical standards

Conflict of interest The authors declare no competing financial interests.

References

- Atkinson BN, Bell SC, De Vivo M, Kowalski LR, Lechner SM, Ognyanov VI, Tham CS, Tsai C, Jia J, Ashton D et al (2001) ALX 5407: a potent, selective inhibitor of the hGlyT1 glycine transporter. *Mol Pharmacol* Dec 60:1414–1420
- Cubelos B, Gimenez C, Zafra F (2005) Localization of the GLYT1 glycine transporter at glutamatergic synapses in the rat brain. *Cereb Cortex* 15:448–459
- Deans MR, Volgyi B, Goodenough DA, Bloomfield SA, Paul DL (2002) Connexin36 is essential for transmission of rod-mediated visual signals in the mammalian retina. *Neuron* 36:703–712
- Dick O, Hack I, Altmann WD, Garner CC, Gundelfinger ED, Brandstätter JH (2001) Localization of the presynaptic cytomatrix protein Piccolo at ribbon and conventional synapses in the rat retina: comparison with Bassoon. *J Comp Neurol* 439:224–234
- Dingledine R, Kleckner NW, McBain CJ (1990) The glycine coagonist site of the NMDA receptor. *Adv Exp Med Biol* 268:17–26
- Dumitrescu ON, Protti DA, Majumdar S, Zeilhofer HU, Wässle H (2006) Ionotropic glutamate receptors of amacrine cells of the mouse retina. *Vis Neurosci* 23:79–90
- Dutertre S, Becker CM, Betz H (2012) Inhibitory glycine receptors: an update. *J Biol Chem* 287:40216–40223
- Eulenburg V, Becker K, Gomez J, Schmitt B, Becker CM, Betz H (2006) Mutations within the human GLYT2 (SLC6A5) gene associated with hyperekplexia. *Biochem Biophys Res Commun* 348:400–405

- Eulenburg V, Retiounskaia M, Papadopoulos T, Gomeza J, Betz H (2010) Glial glycine transporter 1 function is essential for early postnatal survival but dispensable in adult mice. *Glia* Jul 58:1066–1073 (Epub 2010/05/15)
- Farley FW, Soriano P, Steffen LS, Dymecki SM (2000) Widespread recombinase expression using FLPeR (flipper) mice. *Genesis* 28:106–110
- Gomez J, Hulsmann S, Ohno K, Eulenburg V, Szoke K, Richter D, Betz H (2003a) Inactivation of the glycine transporter 1 gene discloses vital role of glial glycine uptake in glycinergic inhibition. *Neuron* 40:785–796
- Gomez J, Ohno K, Hulsmann S, Armsen W, Eulenburg V, Richter DW, Laube B, Betz H (2003b) Deletion of the mouse glycine transporter 2 results in a hyperekplexia phenotype and postnatal lethality. *Neuron* 40:797–806
- Haverkamp S, Wässle H (2000) Immunocytochemical analysis of the mouse retina. *J Comp Neurol* 424:1–23
- Ishihara N, Armsen W, Papadopoulos T, Betz H, Eulenburg V (2010) Generation of a mouse line expressing Cre recombinase in glycinergic interneurons. *Genesis* 48:437–445
- Kurolap A, Armbruster A, Hershkovitz T, Hauf K, Mory A, Paperna T, Hannappel E, Tal G, Nijem Y, Sella E et al (2016) Loss of glycine transporter 1 causes a subtype of glycine encephalopathy with arthrogryposis and mildly elevated cerebrospinal fluid glycine. *Am J Hum Genet* 99:1172–1180
- Latal AT, Kremer T, Gomez J, Eulenburg V, Hulsmann S (2010) Development of synaptic inhibition in glycine transporter 2 deficient mice. *Mol Cell Neurosci* 44:342–352 (Epub 2010/05/08)
- Lee EJ, Kim HJ, Lim EJ, Kim IB, Kang WS, Oh SJ, Rickman DW, Chung JW, Chun MH (2004) AII amacrine cells in the mammalian retina show disabled-1 immunoreactivity. *J Comp Neurol* 470:372–381
- Lee SC, Meyer A, Schubert T, Huser L, Dedek K, Haverkamp S (2015) Morphology and connectivity of the small bistratified A8 amacrine cell in the mouse retina. *J Comp Neurol* 523:1529–1547
- Legendre P (2001) The glycinergic inhibitory synapse. *Cell Mol Life Sci* 58:760–793
- Maxeiner S, Dedek K, Janssen-Bienhold U, Ammermuller J, Brune H, Kirsch T, Pieper M, Degen J, Kruger O, Willecke K et al (2005) Deletion of connexin45 in mouse retinal neurons disrupts the rod/cone signaling pathway between AII amacrine and ON cone bipolar cells and leads to impaired visual transmission. *J Neurosci* 25:566–576
- McIntire SL, Reimer RJ, Schuske K, Edwards RH, Jorgensen EM (1997) Identification and characterization of the vesicular GABA transporter. *Nature* 389:870–876
- Nelson R, Famiglietti Jr EV, Kolb H (1978) Intracellular staining reveals different levels of stratification for on- and off-center ganglion cells in cat retina. *J Neurophysiol* 41:472–483
- Pfeiffer F, Simler R, Grenningloh G, Betz H (1984) Monoclonal antibodies and peptide mapping reveal structural similarities between the subunits of the glycine receptor of rat spinal cord. *Proc Natl Acad Sci USA* 81:7224–7227
- Pourcho RG, Goebel DJ (1985) A combined Golgi and autoradiographic study of (3H)glycine-accumulating amacrine cells in the cat retina. *J Comp Neurol* 233:473–480
- Pow DV (1998) Transport is the primary determinant of glycine content in retinal neurons. *J Neurochem* 70:2628–2636
- Pow DV, Hendrickson AE (1999) Distribution of the glycine transporter glyt-1 in mammalian and nonmammalian retinae. *Vis Neurosci* 16:231–239
- Pow DV, Hendrickson AE (2000) Expression of glycine and the glycine transporter Glyt-1 in the developing rat retina. *Vis Neurosci* 17:1R–9R
- Protti DA, Flores-Herr N, Li W, Massey SC, Wässle H (2005) Light signaling in scotopic conditions in the rabbit, mouse and rat retina: a physiological and anatomical study. *J Neurophysiol* 93:3479–3488 (Epub 2004/12/17)
- Rees MI, Harvey K, Pearce BR, Chung SK, Duguid IC, Thomas P, Beatty S, Graham GE, Armstrong L, Shiang R et al (2006) Mutations in the gene encoding GlyT2 (SLC6A5) define a presynaptic component of human startle disease. *Nat Genet* 38:801–806
- Regus-Leidig H, Ott C, Lohner M, Atorf J, Fuchs M, Sedmak T, Kremers J, Fejtova A, Gundelfinger ED, Brandstätter JH (2013) Identification and immunocytochemical characterization of Piccolino, a novel Piccolo splice variant selectively expressed at sensory ribbon synapses of the eye and ear. *PLoS One* 8:e70373
- Rice DS, Curran T (2000) Disabled-1 is expressed in type AII amacrine cells in the mouse retina. *J Comp Neurol* 424:327–338
- Rousseau F, Aubrey KR, Supplisson S (2008) The glycine transporter GlyT2 controls the dynamics of synaptic vesicle refilling in inhibitory spinal cord neurons. *J Neurosci* 28:9755–9768
- Roux MJ, Supplisson S (2000) Neuronal and glial glycine transporters have different stoichiometries. *Neuron* 25:373–383
- Roux MJ, Martinez-Maza R, Le Goff A, Lopez-Corcuera B, Aragon C, Supplisson S (2001) The glial and the neuronal glycine transporters differ in their reactivity to sulfhydryl reagents. *J Biol Chem* 276:17699–17705
- Sagne C, El Mestikawy S, Isambert MF, Hamon M, Henry JP, Giros B, Gasnier B (1997) Cloning of a functional vesicular GABA and glycine transporter by screening of genome databases. *FEBS Lett* 417:177–183
- Schlosser L, Barthel F, Brandenburger T, Neumann E, Bauer I, Eulenburg V, Werdehausen R, Hermanns H (2015) Glycine transporter GlyT1, but not GlyT2, is expressed in rat dorsal root ganglion—possible implications for neuropathic pain. *Neurosci Lett* 600:213–219
- Schneider CA, Rasband WS, Eliceiri KW (2012) NIH Image to ImageJ: 25 years of image analysis. *Nat Methods* 9:671–675
- Supplisson S, Roux MJ (2002) Why glycine transporters have different stoichiometries. *FEBS Lett* 529:93–101
- Vaney DI, Nelson JC, Pow DV (1998) Neurotransmitter coupling through gap junctions in the retina. *J Neurosci* 18:10594–10602
- Wässle H (2004) Parallel processing in the mammalian retina. *Nat Rev Neurosci* 5:747–757
- Yee BK, Balic E, Singer P et al (2006) Disruption of glycine transporter 1 restricted to forebrain neurons is associated with a procognitive and antipsychotic phenotypic profile. *J Neurosci* 26:3169–3181. <https://doi.org/10.1523/JNEUROSCI.5120-05.2006>
- Zafra F, Aragon C, Olivares L, Danbolt NC, Gimenez C, Storm-Mathisen J (1995) Glycine transporters are differentially expressed among CNS cells. *J Neurosci* 15:3952–3969
- Zeilhofer HU, Studler B, Arabadzisz D, Schweizer C, Ahmadi S, Layh B, Bosl MR, Fritschy JM (2005) Glycinergic neurons expressing enhanced green fluorescent protein in bacterial artificial chromosome transgenic mice. *J Comp Neurol* 482:123–141